

# The Inert Doublet Model and LEP II Limits

Erik Lundström\*

*Department of Physics, Stockholm University, AlbaNova University Center, SE - 106 91 Stockholm, Sweden*

Michael Gustafsson†

*INFN, Sezione di Padova, Department of Physics ‘Galileo Galilei’, Via Marzolo 8, I-35131, Padua, Italy and  
Department of Physics, Stockholm University, AlbaNova University Center, SE - 106 91 Stockholm, Sweden*

Joakim Edsjö‡

*Department of Physics, Stockholm University, AlbaNova University Center, SE - 106 91 Stockholm, Sweden*

The Inert Doublet Model is a minimal extension of the Standard Model introducing an additional SU(2) doublet with new scalar particles that could be produced at accelerators. While there exists no LEP II analysis dedicated for these inert scalars, the absence of a signal within searches for supersymmetric neutralinos can be used to constrain the Inert Doublet Model. This translation however requires some care because of the different properties of the inert scalars and the neutralinos. We investigate what restrictions an existing DELPHI collaboration study of neutralino pair production can put on the inert scalars, and discuss the result in connection with dark matter. We find that although an important part of the Inert Doublet Model parameter space can be excluded by the LEP II data, the lightest inert particle still constitutes a valid dark matter candidate.

## I. INTRODUCTION

The Inert Doublet Model (IDM) extension of the particle Standard Model has recently attracted attention within the particle physics and cosmology community. Despite its simplicity - a two Higgs doublet model with an imposed unbroken  $Z_2$  parity - it displays a remarkably rich phenomenology. After being touched upon already in the 1970s [1] the model has in later years been studied within various contexts such as light neutrino generation [2, 3], leptogenesis [3], Higgs phenomenology [4, 5], improved naturalness [4, 6], electroweak symmetry breaking [7], and as a dark matter candidate [2, 3, 4, 8, 9].

Besides the Standard Model-like Higgs boson,  $h$ , the IDM contains three additional scalar fields: two neutral,  $H^0$  and  $A^0$ , and one charged,  $H^\pm$ . Because of the exact  $Z_2$  parity none of the new particles have direct (Yukawa-) couplings to fermions and are hence called *inert* scalars (or sometimes even inert Higgs bosons [4, 9]). Because the new doublet still couples directly to  $h$  and the gauge bosons (and does not generate Standard Model masses) some have preferred to instead denote the model the Dark Scalar Doublet Model (DSDM) [5].

The  $Z_2$  parity also ensures the stability of the Lightest Inert Particle (LIP), which hence, if it is either  $H^0$  or  $A^0$ , constitutes a good dark matter candidate belonging to the class of Weakly Interacting Massive Particles (WIMPs). For masses below 80 GeV it can leave a relic abundance in agreement with the WMAP constraints [10, 11] and hence explain all the dark matter [4, 8, 9].

Another striking property of the IDM is that it can

allow for a heavy ( $\sim 500$  GeV) Standard Model Higgs boson  $h$  without violating data from electroweak precision tests [4]. Although the direct Higgs searches are not in conflict with the 95% C.L. upper Higgs mass bound set by the precision tests (assuming only Standard Model physics), they are well above the indicated central value [12]. If upcoming accelerator searches fail to detect a light ( $\lesssim 200$  GeV) Higgs boson the IDM may constitute an attractive explanation.

Although the IDM (in contrast to *e.g.* supersymmetric models) seems to lack any deeper fundamental motivations, its strength instead lies in its simplicity, and the model can be regarded as an archetype for more comprehensive extensions of the Standard Model (like [13] or [14]). Just like generic spin-1/2 and spin-1 WIMPs could be represented by the supersymmetric neutralino and the first Kaluza-Klein excitation of the photon, respectively, the lightest inert particle could be used as a representative of spin-0 WIMP dark matter candidates.

Experimental bounds and signatures of the IDM have been investigated in several papers. Studies show that the WIMP-nucleon scattering cross section in general lies below the sensitivity of current deep underground direct detection experiments [4, 8]. The prospects for indirect detection via gamma-rays produced in dark matter self-annihilation processes in the galactic halo look more promising [8, 9, 15], especially since inert scalar dark matter has the ability to produce extraordinarily clear spectral lines [9]. LEP I data on the width of the  $Z$  boson force the sum of the  $H^0$  and  $A^0$  masses to be larger than the  $Z$  mass [5, 9], while the LEP electroweak precision tests put constraints on the inert scalar mass splittings as a function of the  $h$  mass [4]. Moreover, detection at the LHC seems feasible [5].

What has been missing so far in the investigation of the IDM is a closer study in connection with the existing LEP II data. So far the LEP II limits on the IDM are

---

\*Electronic address: erik@physto.se

†Electronic address: gustafss@pd.infn.it

‡Electronic address: edsjo@physto.se

only rough estimates based on direct usage of production cross section limits from existing analyses of the Minimal Supersymmetric Standard Model (MSSM) [4, 13]. Although this may be suitable as a first approximation, there are certainly some important differences between the IDM and the MSSM which threaten to alter the conclusions.

In this paper we take a closer look at the limits LEP II data can set on the IDM. We make use of an existing DELPHI collaboration study of neutralino pair production [16] where detailed signals and backgrounds have already been simulated. By generating  $H^0 A^0$  events and mimicking the cuts performed on the dataset in [16], we can estimate upper limits on the corresponding production cross sections. These limits are then used to constrain the masses of the inert scalars.

The outline of the paper is as follows: In Section II we present the IDM setup in more detail and discuss its theoretical and experimental constraints. In Section III we motivate the need for a more careful LEP II analysis, and introduce the method used here to constrain the IDM parameter space. In Section IV we present the results, and discuss those in connection with dark matter. Section V includes some final remarks and conclusions. A short summary of this paper is given in Section VI. Appendices A and B provide detailed lists of the cuts used for the acoplanar jets and acoplanar leptons selections, respectively.

## II. THE INERT DOUBLET MODEL

### A. Description

Although electroweak symmetry breaking can be achieved with a single Higgs doublet, a more complicated Higgs sector is not excluded. Since problems like dark matter and neutrino mass generation seem to require new physics beyond the Standard Model, minimal extensions could be considered as attractive models compatible with the principle of Occam's razor.

A simple and well known extension of the Standard Model Higgs sector is the Two Higgs Doublet Model (THDM), in which there exist two scalar doublets,  $H_1$  and  $H_2$ . In order not to be in conflict with the tight constraints on the magnitude of flavor changing neutral currents a  $Z_2$  parity, under which  $H_1 \rightarrow H_1$  and  $H_2 \rightarrow -H_2$ , is imposed. The most general renormalizable and CP conserving potential of such a model is

$$V = \mu_1^2 |H_1|^2 + \mu_2^2 |H_2|^2 + \lambda_1 |H_1|^4 + \lambda_2 |H_2|^4 + \lambda_3 |H_1|^2 |H_2|^2 + \lambda_4 |H_1^\dagger H_2|^2 + \lambda_5 \text{Re} \left[ (H_1^\dagger H_2)^2 \right], \quad (1)$$

where  $\mu_i^2$  and  $\lambda_i$  are real parameters. Whether the Higgs doublets develop vacuum expectation values (vevs) or not of course depends on the values of the parameters in the potential [1]. Even if one usually assumes that both dou-

blets develop vevs, there is a priori nothing which requires that phase.

The IDM is a THDM where only one of the Higgs doublets,  $H_1$ , acquires a vev,  $v$ . Hence,  $H_1$  closely corresponds to the ordinary Standard Model Higgs doublet. Moreover, the IDM belongs to the class of Type I THDMs in which all Standard Model fields are taken to be  $Z_2$  even. As a consequence no Yukawa terms including  $H_2$  are allowed by the symmetry. The nonexistence of a vev,  $v_2$ , for  $H_2$  leaves the imposed  $Z_2$  parity unbroken and ensures the absence of mixing between the components of  $H_1$  and those of  $H_2$ . Thus, the fields belonging to  $H_2$  are inert in the sense that they do not couple directly to fermions, and the lightest of them is automatically stable. It should be noted that the IDM is not the  $v_2 \rightarrow 0$  limit of a THDM in which both Higgs doublets develop vevs.

After giving masses to the gauge bosons,  $H_1$  has one physical degree of freedom left: the real scalar field  $h$ . Since  $h$  closely resembles the Higgs particle of the Standard Model it will here be called the Standard Model Higgs boson. In addition,  $H_2$  includes the neutral CP-even  $H^0$ , the neutral CP-odd  $A^0$ , and the charged  $H^\pm$  inert scalars. The masses of the particles are (at tree level) given by

$$\begin{aligned} m_h^2 &= -2\mu_1^2, \\ m_{H^0}^2 &= \mu_2^2 + (\lambda_3 + \lambda_4 + \lambda_5)v^2, \\ m_{A^0}^2 &= \mu_2^2 + (\lambda_3 + \lambda_4 - \lambda_5)v^2, \\ m_{H^\pm}^2 &= \mu_2^2 + \lambda_3 v^2, \end{aligned} \quad (2)$$

where  $v = m_h/\sqrt{4\lambda_1}$  is the vev of  $H_1$ . (The measured gauge boson masses determine  $v \approx 175$  GeV.)

If either of the electrically neutral  $H^0$  or  $A^0$  constitutes the lightest inert particle, it could be a good WIMP dark matter candidate. By assuming  $m_{H^0} < m_{A^0}$  we will from now on have  $H^0$  as our potential dark matter particle, although the roles of  $H^0$  and  $A^0$  are in general interchangeable.

The mass difference between the  $A^0$  and  $H^0$  is frequently appearing in calculations, and for later convenience we define

$$\Delta m \equiv m_{A^0} - m_{H^0}. \quad (3)$$

### B. Constraints

The requirements of vacuum stability and perturbativity set theoretical constraints on the model. If and only if

$$\begin{aligned} \lambda_{1,2} &> 0 \\ \lambda_3, \lambda_3 + \lambda_4 - |\lambda_5| &> -2\sqrt{\lambda_1 \lambda_2} \end{aligned} \quad (4)$$

the potential  $V$  of Eq. (1) is bounded from below, ensuring a stable vacuum. We will follow [4] and adopt

$$\begin{aligned} \lambda_3^2 + (\lambda_3 + \lambda_4)^2 + \lambda_5^2 &< 12\lambda_1^2 \\ \lambda_2 &< 1 \end{aligned} \quad (5)$$

as sufficient conditions for a perturbatively well-behaved model.

Observational constraints come from direct and indirect detection experiments, measurements of the cosmic microwave background, and accelerator searches.

The absence of WIMP-nucleon scattering signals in existing direct detection experiments disfavors models very close to having a Peccei-Quinn symmetry  $m_{H^0} = m_{A^0}$  [4], but otherwise direct detection cannot currently put any important constraints on the IDM parameter space [4, 8].

Indirect detection through gamma-rays produced by annihilating  $H^0$  pairs in and around the galactic center has been studied in several papers [8, 9, 15]. Although IDM models (with  $m_{H^0} < m_W$  and large values of  $m_h$ ) have been shown capable of producing spectacularly clear monochromatic line signals [9], the absolute photon fluxes are subject to large astrophysical uncertainties. Also, the most interesting photon energy range has not yet been covered (but is currently examined by the Fermi Gamma-ray Space Telescope [17]). Thus it is not yet possible to derive any robust constraints from indirect detection.

The WMAP data on the cosmic microwave background radiation limits the relic abundance of dark matter,  $\Omega_{DM}$ , to  $0.094 < \Omega_{DM} h^2 < 0.129$  [10], where  $h$  is the Hubble constant in units of  $100 \text{ km Mpc}^{-1} \text{ s}^{-1}$ . The lower bound need only be respected if the IDM alone is to solve the dark matter problem. However, the relic density of  $H^0$  particles must always respect the upper bound, since they otherwise would overclose the universe.

While the electroweak precision tests in the absence of new physics beyond the Standard Model favor a light Higgs boson, this does not remain true once the inert scalars are taken into account. In [4] it was shown that the inert particles make important contributions to the electroweak observable  $T$  according to

$$\Delta T \approx \frac{1}{24\pi^2 \alpha v^2} (m_{H^\pm} - m_{A^0}) (m_{H^\pm} - m_{H^0}), \quad (6)$$

where  $\alpha$  is the fine-structure constant. With appropriate inert scalar mass splittings the IDM can hence compensate for too small value of  $T$  arising for heavy Standard Model Higgs boson. From Fig. 1 in [4] we have estimated the allowed  $\Delta T$  range (at 68% C.L.) as a function of  $m_h$ . Together with Eq. (6) this translates into the constraint

$$\begin{aligned} (m_{H^\pm} - m_{A^0}) (m_{H^\pm} - m_{H^0}) \\ \approx 24\pi^2 \alpha v^2 \left[ 0.15 \ln \left( \frac{m_h}{m_Z} \right) \pm 0.1 \right]. \end{aligned} \quad (7)$$

As first noted in [9] and more explicitly argued in [5] the precise LEP I measurements of the  $Z$  boson width forbids the decay channel  $Z \rightarrow H^0 A^0$ . Hence it is required that

$$m_{H^0} + m_{A^0} > m_Z. \quad (8)$$

When it comes to limits set by the LEP II experiments, previous studies have provided rough estimates based on existing analyses for neutralinos,  $\tilde{\chi}_i^0$ , within the MSSM. By simply applying the same upper limits on the  $e^+e^- \rightarrow H^0 A^0$  cross section as those set by the different LEP collaborations on  $\tilde{\chi}_1^0 \tilde{\chi}_2^0$  production, one finds that the LEP II data seem capable of ruling out important parts of the parameter space. [4, 13]. These observations bring up the question of what restrictions a more specific study of  $H^0 A^0$  production could put on the IDM parameter space.

### III. LEP II ANALYSIS

#### A. Motivation

Although a complete analysis including optimization of cuts, a detailed detector simulation and Standard Model background event generation would put the most accurate LEP II limits on the IDM, it also demands a lot of effort to be carried out. On the other hand, the earlier estimates of LEP II constraints [4, 13] are quite coarse and, as motivated below, need to be improved (or possibly verified). In this work we have therefore chosen to reuse cuts, detector acceptances, simulated backgrounds and derived production cross section limits from an existing MSSM analysis [16], and instead focus on IDM signal event generation and efficiency determination. This method, which will be described in detail in Section III B, is careful enough to put more accurate limits than the current existing estimates.

The different LEP experiments have separately searched for neutralinos via the production process  $e^+e^- \rightarrow \tilde{\chi}_1^0 \tilde{\chi}_2^0$  followed by the decay  $\tilde{\chi}_2^0 \rightarrow \tilde{\chi}_1^0 f \bar{f}$  [18, 19, 20, 21]. The lightest neutralino,  $\tilde{\chi}_1^0$ , is assumed to be stable and would show up as missing energy, while the fermion pair,  $f \bar{f}$ , could be detected as acollinear jets or leptons.

As noted in [5], there are several reasons why the limits derived for  $\tilde{\chi}_1^0 \tilde{\chi}_2^0$  production need not apply to  $H^0 A^0$  production. The inert particles are scalars while the neutralinos carry spin 1/2, and in principle spin correlation effects could make a difference. The production of  $H^0 A^0$  pairs only proceeds via s-channel spin-1  $Z$  bosons,  $e^+e^- \rightarrow Z \rightarrow H^0 A^0$ , forcing the spinless outgoing scalars into states with large transverse momentum, while neutralinos have the ability to conserve angular momentum with the help of their intrinsic spin. Moreover, neutralino production differs in that it can also take place via t-channel selectron exchange. Similarly,  $A^0$  only decays according to  $A^0 \rightarrow H^0 Z \rightarrow H^0 f \bar{f}$ , while both  $\tilde{\chi}_2^0 \rightarrow \tilde{\chi}_1^0 Z \rightarrow \tilde{\chi}_1^0 f \bar{f}$  and  $\tilde{\chi}_2^0 \rightarrow \tilde{f} \tilde{f} \rightarrow \tilde{\chi}_1^0 f \bar{f}$  are allowed (where  $\tilde{f}$  denotes a sfermion). Figs. 1(a)-(d) and Figs. 2(a)-(b) show Feynman diagrams contributing to the production and decay processes. In summary, there are many effects which threaten to spoil a simple direct translation of the LEP II limits derived for the MSSM.

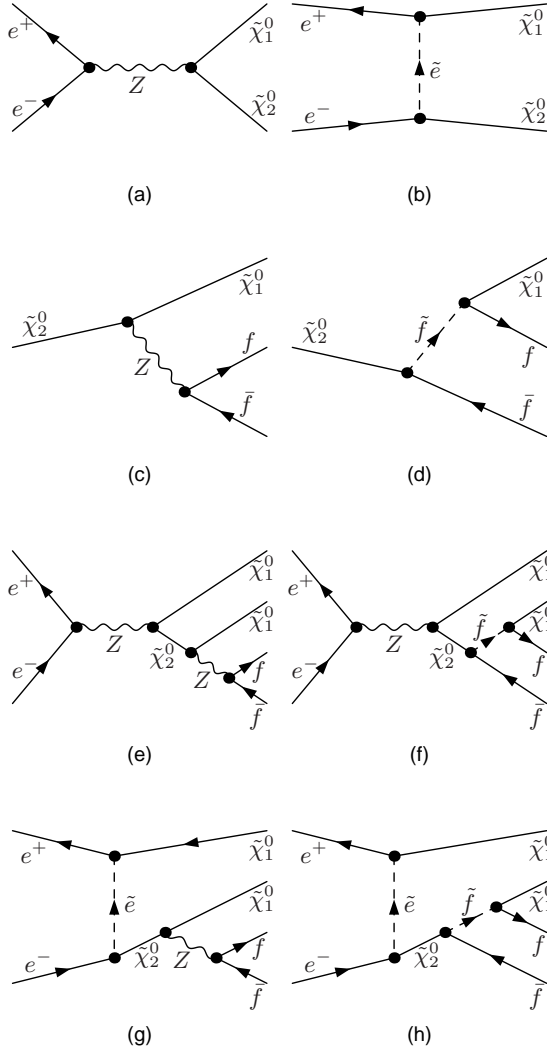


FIG. 1: Representative Feynman diagrams contributing to  $\tilde{\chi}_1^0 \tilde{\chi}_2^0$  events at LEP. Figures (a)-(d) show the process factorized into  $e^+e^- \rightarrow \tilde{\chi}_1^0 \tilde{\chi}_2^0$  production, (a) and (b), and subsequent  $\tilde{\chi}_2^0 \rightarrow \tilde{\chi}_1^0 f \bar{f}$  decay, (c) and (d). Figures (e)-(h) show the unfactorized process  $e^+e^- \rightarrow \tilde{\chi}_1^0 \tilde{\chi}_2^0 \rightarrow \tilde{\chi}_1^0 \tilde{\chi}_1^0 f \bar{f}$ .

To illustrate observable outcomes we take help of the event generator MADGRAPH/MADEVENT [22], which is to be further discussed in Section III B. A comparison between the angular distributions of  $e^+e^- \rightarrow \tilde{\chi}_1^0 \tilde{\chi}_2^0$  and  $e^+e^- \rightarrow H^0 A^0$  indicates that there are significant differences between the two processes. Fig. 3 shows the angular probability distribution of produced  $\tilde{\chi}_2^0$  and  $A^0$  for representative models with various neutralino and inert scalar masses. As can be seen,  $A^0$  is mainly produced with large transverse momentum, while the  $\tilde{\chi}_2^0$  distribution is closer to isotropic.

Once including the decay processes one would expect the angular distribution of final state particles to get a bit smeared out. In order to properly include spin correlation and off-shell effects the full  $e^+e^- \rightarrow \tilde{\chi}_1^0 \tilde{\chi}_2^0 \rightarrow \tilde{\chi}_1^0 \tilde{\chi}_1^0 f \bar{f}$  and  $e^+e^- \rightarrow H^0 A^0 \rightarrow H^0 H^0 f \bar{f}$  matrix elements, shown

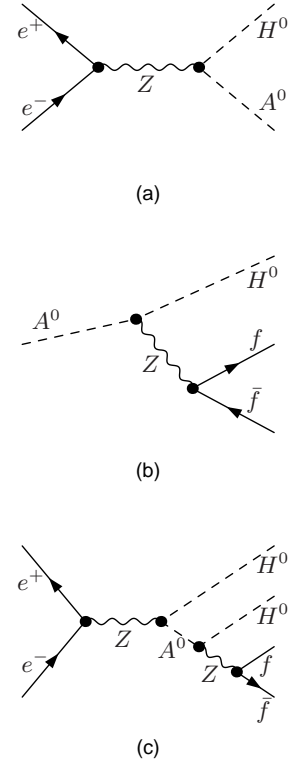


FIG. 2: Feynman diagrams contributing to  $H^0 A^0$  events at LEP. Figures (a) and (b) show the process factorized into  $e^+e^- \rightarrow H^0 A^0$  production, (a), and subsequent  $A^0 \rightarrow H^0 f \bar{f}$  decay, (b). Figure (c) shows the unfactorized process  $e^+e^- \rightarrow H^0 A^0 \rightarrow H^0 H^0 f \bar{f}$ .

in Figs. 1(e)-(h) and Fig. 2(c), have to be calculated without factorizing them into production ( $e^+e^- \rightarrow \tilde{\chi}_1^0 \tilde{\chi}_2^0$ ,  $e^+e^- \rightarrow H^0 A^0$ ) and decay ( $\tilde{\chi}_2^0 \rightarrow \tilde{\chi}_1^0 f \bar{f}$ ,  $A^0 \rightarrow H^0 f \bar{f}$ ) parts (see *e.g.* [23]). However, the analysis of [16] does not include any spin correlation effects and we hence focus on the factorized  $e^+e^- \rightarrow \tilde{\chi}_1^0 \tilde{\chi}_2^0$ ,  $\tilde{\chi}_2^0 \rightarrow \tilde{\chi}_1^0 f \bar{f}$  process, Figs. 1(a)-(d), for the neutralinos. Even if spin correlations are absent for scalars, off-shell effects could in principle make some difference and we hence use the unfactorized process, Fig. 2(c), for the IDM.

Fig. 4 shows the angular probability distribution of the final state fermions for the same models as in Fig. 3. Since we factorize the MSSM processes, and since the inert scalars carry no spin, an isotropic decay in the rest frame of the mother particle ( $\tilde{\chi}_2^0$  or  $A^0$ ) is expected. This makes the final angular distributions considerably flatter, and the MSSM and IDM models typically produce rather similar results, see Figs. 4(b)-(c). However, if the velocity of the mother particle is large and the energy injected into the  $f \bar{f}$  pair during the decay is relatively low, the boost can preserve some significant difference. In other words, the MSSM and IDM final fermion distributions will still differ for models where the center-of-mass energy,  $\sqrt{s}$ , is well above the kinematical limit for neutralino/inert scalar pair production, while at the same time the mass difference between the produced par-

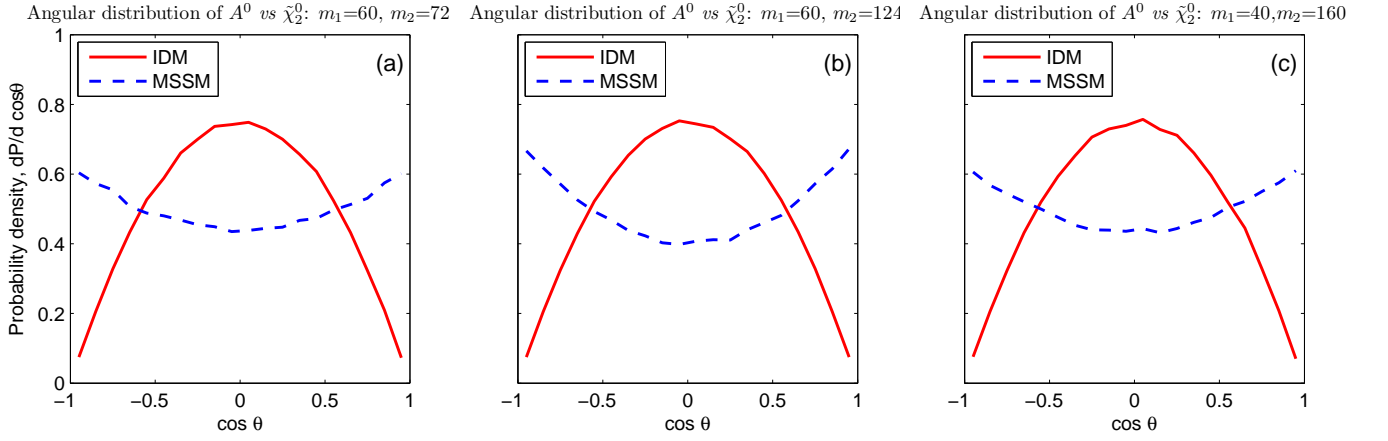


FIG. 3: Angular distribution of  $A^0$  (IDM) versus  $\tilde{\chi}_2^0$  (MSSM) produced in  $e^+e^- \rightarrow \tilde{\chi}_1^0 \tilde{\chi}_2^0$  and  $e^+e^- \rightarrow H^0 A^0$ , respectively. The header of each subfigure displays (in units of GeV) the mass  $m_1$  of  $H^0$  and  $\tilde{\chi}_1^0$ , and the mass  $m_2$  of  $A^0$  and  $\tilde{\chi}_2^0$ . The beam pipe is defined to be along  $\cos \theta = \pm 1$  and the center-of-mass energy is  $\sqrt{s} = 206$  GeV. The large difference between the IDM and the MSSM models is due to the scalar *versus* fermion nature of the outgoing states.

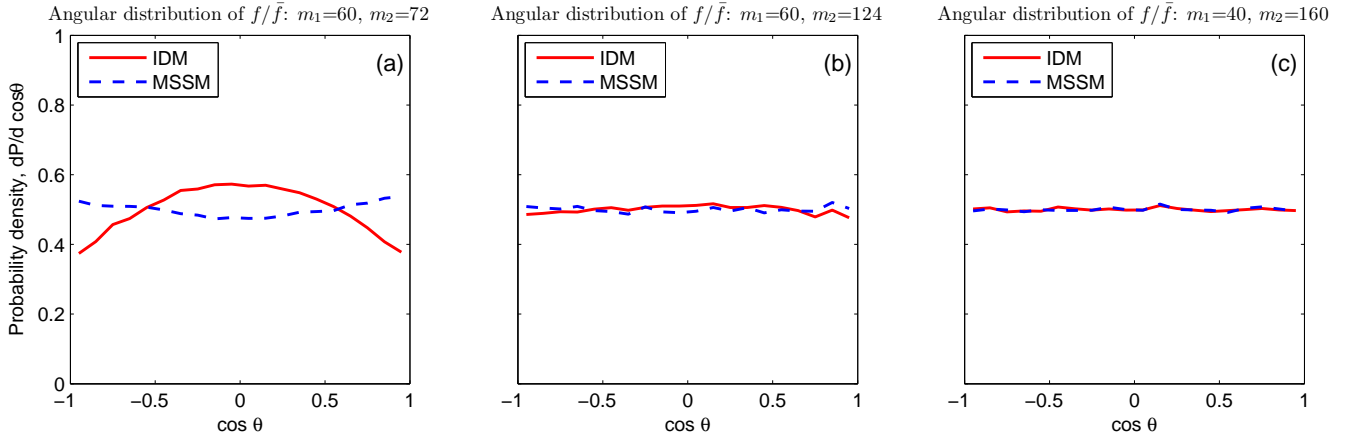


FIG. 4: Angular distribution of final state fermions from  $e^+e^- \rightarrow H^0 A^0 \rightarrow H^0 H^0 f \bar{f}$  (IDM) *versus*  $e^+e^- \rightarrow \tilde{\chi}_1^0 \tilde{\chi}_2^0, \tilde{\chi}_2^0 \rightarrow \tilde{\chi}_1^0 f \bar{f}$  (MSSM). The models are the same as in Fig. 3. In (a) the velocity of the mother particle  $A^0/\tilde{\chi}_2^0$  is large and the energy injected into the fermions during the decay is relatively low, and hence the discrepancy from Fig. 3 can survive.

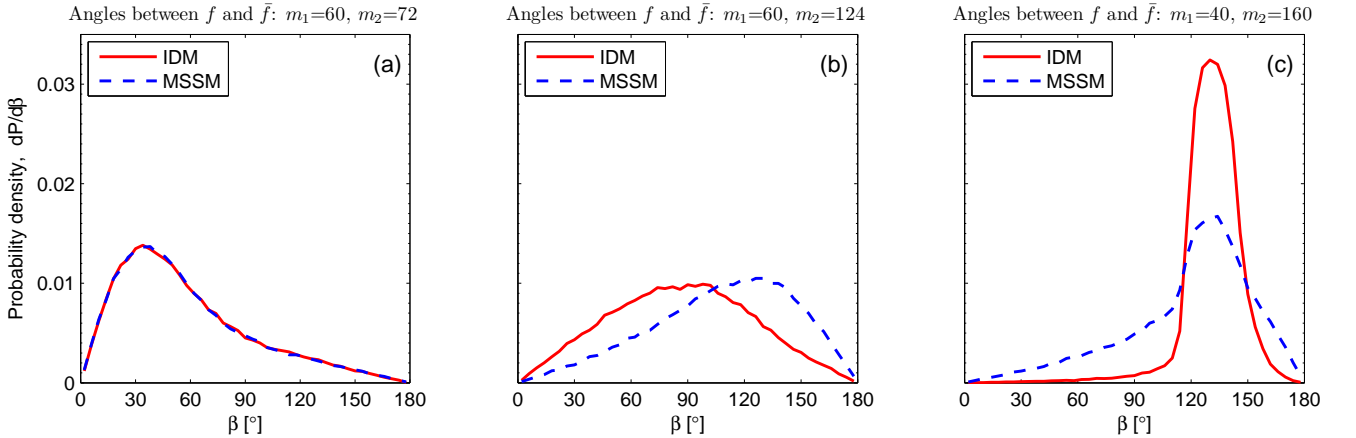


FIG. 5: Fermion opening angle distribution for the same processes and models as in Fig. 4.  $\beta$  is the angle between the two outgoing fermions  $f$  and  $\bar{f}$  as measured in the lab frame. In (a) the IDM and SUSY distributions happen to be overlapping, but one should keep in mind that in the MSSM the decay distribution can depend on the gaugino fraction of  $\tilde{\chi}_2^0$ . Figs. 3-5 are based on  $10^5$  events per model, as generated with MADGRAPH/MADEVENT [22].



ticles is small, see Fig. 4(a). Noteworthy, this is also exactly the interesting dark matter preferred region of rather light  $H^0$  ( $m_{H^0} < m_W$ ) together with a considerable amount of coannihilation ( $\Delta m \lesssim 10$  GeV) [4, 8, 9].

It should be stressed that there are of course other observables than individual scattering angles which may differ between the MSSM and the IDM models. As an example Fig. 5 shows the  $f\bar{f}$  opening angle distributions, where clear differences is seen in Figs. 5(b)-(c). Which observables that are important depends on what cuts are imposed, and in general it can be hard to extract any reliable information without doing a more complete analysis. In any case, it should be clear from the above examples that there exist differences between the MSSM and the IDM which could hinder a direct application of the existing LEP II neutralino production cross section limits on the inert scalars. We therefore find it well motivated to study the LEP II bounds on the IDM more closely.

## B. Method

### 1. General outline

A DELPHI collaboration search for pair production of neutralinos in the center of mass energy range 192–208 GeV [16] forms the base of this paper. In [16] the absence of an excess above the Standard Model background in the DELPHI data was used to put upper limits on neutralino production cross sections. The analysis included a careful Standard Model background generation and a detailed detector simulation. The signal events were produced with the help of SUSYGEN 2.2004 [24], and JETSET 7.4 [25] was used for quark fragmentation. Every event was tested against a number of searches with cuts optimized for different final state topologies, each using a sequential cuts approach. These searches, which are described in detail in [16], were ordered according to: 1) acoplanar jets, 2) acoplanar leptons, 3) multijets, 4) multileptons, and 5) asymmetric taus, and an event being accepted by one of the selections was explicitly rejected by those appearing later in the list. However, the searches were designed to be mutually exclusive in order to substantially reduce the possibility of events being capable of passing more than one of the searches. Based on the resulting efficiencies for simulated signal events, 95% C.L. upper limits on neutralino production cross sections were derived and presented as functions of neutralino masses in contour plots. Of interest for this paper are Figs. 12 and 13 in [16] where  $\tilde{\chi}_1^0 \tilde{\chi}_2^0$  production followed by  $\tilde{\chi}_2^0$  decay into  $\tilde{\chi}_1^0$  plus a fermion pair ( $q\bar{q}$ ,  $\mu^+\mu^-$ ,  $e^+e^-$ , or according to the branching ratios of the  $Z$  boson) was assumed. Direct translation of these kinds of plots is what previously has been used to estimate rough limits on the IDM.

The basic strategy of this work is simple: simulate  $e^+e^- \rightarrow H^0 A^0$  events, pass them through the same cuts as those used in [16] to determine IDM signal efficiencies, and finally rescale the in [16] derived upper limits

on production cross sections in accordance with the ratio between the MSSM and IDM efficiencies. However, in reality the full analysis of [16] is not practically possible to reproduce in full detail. Instead we rely on slightly different codes for event generation, a rough detector simulation, and a somewhat simplified set of cuts. Thus a re-evaluation of also the MSSM efficiencies is required, both for consistency and in order to check the reliability of our method.

### 2. MSSM framework

The free parameters of the R-parity conserving MSSM considered by [16] are  $\tan\beta$ ,  $\mu$ ,  $M_2$ ,  $m_0$ ,  $A$  and  $m_A$ . The gaugino mass parameters  $M_1$  and  $M_2$  are assumed to be related according to the mSUGRA unification relation:  $M_1 \approx 0.5M_2$ . By choosing a high common scalar mass parameter  $m_0 \sim 1$  TeV, [16] put focus on models with sfermions much heavier than the produced neutralinos. For fixed values of  $\tan\beta$  (*i.e.* the ratio between the vacuum expectation values of the two Higgs doublets), [16] performed scans over  $M_2$  and the Higgs mass parameter  $\mu$  to find models with suitable values of the  $\tilde{\chi}_1^0$  and  $\tilde{\chi}_2^0$  masses. The common trilinear coupling  $A$  and the pseudoscalar Higgs mass  $m_A$  typically have no noticeable influence on the results.

Because of the assumed unification relation between  $M_1$  and  $M_2$  there are no models with the mass of  $\tilde{\chi}_2^0$  much larger than twice the mass of  $\tilde{\chi}_1^0$ . Therefore [16] considered  $\tilde{\chi}_1^0 \tilde{\chi}_3^0$  production followed by the decay  $\tilde{\chi}_3^0 \rightarrow \tilde{\chi}_1^0 f \bar{f}$  when they explored larger neutralino mass differences. However, their notation was to not explicitly write out any  $\tilde{\chi}_3^0$ , but instead use  $\tilde{\chi}_2^0$  for any heavier neutralino. We follow the same convention here. Although one can in general find several points within the  $(\tan\beta, M_2, \mu)$  parameter space giving the same set of  $(\tilde{\chi}_1^0, \tilde{\chi}_2^0)$  masses, the differences in efficiencies are typically small.

### 3. Signal generation

For the generation of signal events we use the MADGRAPH/MADEVENT package [22]. There are two main reasons for this choice: 1) It is possible to generate both MSSM and IDM events with MADGRAPH/MADEVENT. 2) The code allows multiparticle final states, giving the opportunity to generate the complete  $2 \rightarrow 4$  processes in one step, thus fully taking spin correlation and off-shell effects into account. In agreement with [16], the MSSM processes are factorized into  $e^+e^- \rightarrow \tilde{\chi}_1^0 \tilde{\chi}_2^0$ , followed by either of  $\tilde{\chi}_2^0 \rightarrow \tilde{\chi}_1^0 q\bar{q}$ ,  $\tilde{\chi}_2^0 \rightarrow \tilde{\chi}_1^0 \mu^+\mu^-$  or  $\tilde{\chi}_2^0 \rightarrow \tilde{\chi}_1^0 e^+e^-$ . The decays are arranged to be isotropic in the rest frame of  $\tilde{\chi}_2^0$ , after which the decay products are boosted into the lab frame. The IDM events, on the other hand, are generated via the unfactorized processes  $e^+e^- \rightarrow H^0 A^0 \rightarrow H^0 H^0 f\bar{f}$ , where  $f\bar{f}$  represents either one of  $q\bar{q}$ ,  $\mu^+\mu^-$  or  $e^+e^-$ . As a consistency check we also study numer-

ous unfactorized MSSM processes as well as factorized IDM processes. Although slight deviations in for example the angular distribution of produced particles can be found between the factorized and unfactorized MSSM processes, the discrepancies left at the level of efficiency determination are quite small. For the IDM this agreement is even better.

We fix the center of mass energy  $\sqrt{s}$  to 206 GeV in our analysis, and note that the final results hardly depend on the exact value.

PYTHIA 6.4 [26] is used for the fragmentation and hadronization of final state quarks, and jets are reconstructed with the PYCLUS algorithm. The minimum transverse jet separation is set to  $d_{join} = 10$  GeV while at the same time requiring at least two reconstructed jets, all in agreement with [16].

#### 4. Cuts

Different cuts are imposed depending on whether the final state includes quark or lepton pairs. We mimic the cuts of the acoplanar jets search and the acoplanar leptons search in [16] as closely as possible, and apply them to the quark and lepton events, respectively. Muon and electron identifications are performed with the help of tabulated acceptances extracted from an earlier detailed study of the DELPHI detector [27]. Given the four-momentum of the lepton, a probability for identification is assigned and used to generate identification status.

Because of *e.g.* our lack of a detailed detector simulation, some of the cuts have to be somewhat simplified, and some are not even possible to carry out. However, much effort has been put into accounting for all major effects in order to assure the reliability of our final conclusions.

In principle an event not passing the acoplanar jets or acoplanar leptons cuts could instead happen to be accepted by one of the subsequent searches (*i.e.* the multi-jets, multileptons or asymmetric taus selections). Owing to the design of the searches we expect these events to be quite rare, and that the relative MSSM and IDM efficiencies in any case can be fairly represented by the corresponding results from the acoplanar searches. We therefore only impose one set of cuts on each event: the acoplanar jets (for  $q\bar{q}$  final states) or the acoplanar leptons (for  $\mu^+\mu^-$  and  $e^+e^-$  final states) selections. The exact selection cuts are described in Appendix A and Appendix B.

#### 5. Calculating efficiencies

We start our analysis by generating (on average a handful of different) MSSM models for each set of  $(\tilde{\chi}_1^0, \tilde{\chi}_2^0)$  masses considered. We create the models using the spectrum generator SUSPECT 2.34 [28] and feed the results into MADGRAPH/MADEVENT to simulate MSSM

events. In total we generate more than 15 million  $\tilde{\chi}_1^0\tilde{\chi}_2^0$  events distributed among roughly 200 different MSSM models. Efficiencies are then calculated by passing the generated events through our cuts. As a reliability check of our analysis, the found efficiencies are compared with those of Table 8 in [16]. Although an exact agreement is too much to demand, the ratios between our calculated efficiencies and those in [16] should at least stay rather constant for all  $(\tilde{\chi}_1^0, \tilde{\chi}_2^0)$  mass points. Indeed we find that this ratio stays in the interval 0.7–1.0 for most models, a result accurate enough for our needs. Some deviations occur, but this happens mainly in not very important regions of the parameter space, and can possibly be understood by taking into account the uncertainties in the jet energy determination by the true detector. See Section V for further discussion.

Within the IDM the cross sections for production of  $H^0A^0$  events are on the other hand completely specified once  $m_{H^0}$  and  $m_{A^0}$  are given, and hence only one model for each set of  $(H^0, A^0)$  masses needs to be examined. Again MADGRAPH/MADEVENT is used to simulate (about four million) signal events, which are subsequently taken through the same cuts in order to extract the corresponding IDM efficiencies.

#### 6. Constraining the IDM

We can now determine the ratio between our calculated MSSM and IDM efficiencies as a function of the produced neutralino/inert scalar masses. These are then used to rescale the cross section upper limits presented in [16]. It should be noted that although the 14 mass combinations given in Table 8 in [16] serve as our starting check points, we investigate many more to cover the complete  $(m_{H^0}, m_{A^0})$  plane and to be more detailed around more critical regions.

In the decay of  $A^0$ , fermion pairs are produced at tree level via s-channel  $Z$  bosons, and the branching ratios into fermions are therefore expected to be close to these of an on-shell  $Z$  boson. It is therefore natural to focus on the cross section limits provided by Fig. 13d) in [16], where the final fermions are assumed to be produced in accordance to the branching ratios of the  $Z$  boson. This is clearly appropriate for models with a large mass splitting  $\Delta m$  (and specifically when  $\Delta m \geq m_Z$  so that  $Z$  is real), but some modifications may be needed for models where the intermediate  $Z$  boson is very virtual and the branching may be somewhat different. In other words, when  $\Delta m$  is small we need to evaluate the branching ratios to find out whether some modifications might be needed (this calculation is done with MADGRAPH/MADEVENT).

Finally, we calculate the  $H^0A^0$  production cross section as a function of  $m_{H^0}$  and  $m_{A^0}$ , and compare it with our derived cross section upper limits in order to constrain the IDM parameter space.

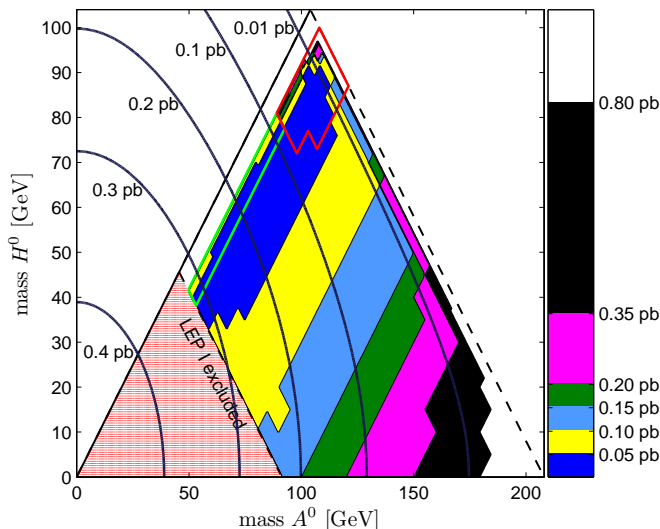


FIG. 6: Production cross section upper limits as extracted from Fig. 13d) in [16]. For models inside the red (green) contour the limits are rescaled by a factor 0.9 (1.1) before being applied to  $H^0 A^0$  production. The dark blue contour lines indicate the  $e^+ e^- \rightarrow H^0 A^0$  cross section. The red region where  $m_{H^0} + m_{A^0} < m_Z$ , is excluded by LEP I data on the Z boson width. The upper right dashed line shows the LEP II kinematical limit.

#### IV. RESULTS

Under our imposed cuts the resulting IDM and MSSM efficiencies turn out to be quite similar, an appealing, although not at all trivial, result.

The efficiencies are first determined for each individual channel ( $q\bar{q}$ ,  $\mu^+ \mu^-$ ,  $e^+ e^-$ ), after which those are combined into an efficiency representing the true branching ratio. This combination is done by weighting the channels in accordance with the decay branching ratios of the Z boson (*i.e.* the  $q\bar{q}$  efficiency is given the highest weight).

We find that whenever  $m_{H^0} \lesssim 80$  GeV the IDM efficiencies typically are a few percent higher than those of the corresponding MSSM models. An important observation is that we find no mass combinations in this region where the MSSM gives a higher efficiency than the IDM, and it is therefore appropriate to apply at least as hard production cross section upper limits on the inert scalars as those put on the neutralinos in [16].

In the specific region defined by  $8 \text{ GeV} < \Delta m < 15 \text{ GeV}$  and  $m_{H^0} \lesssim 85 \text{ GeV}$ , the IDM efficiencies are found to be about a factor 1.15-1.20 higher than those of the MSSM. On noting that the models with the lowest  $\Delta m$  has a slightly higher branching into neutrinos compared to ordinary Z boson decay, we in this region adopt a conservative factor of 0.9 with which we rescale the neutralino production limits given in Fig. 13d) in [16]. This region is encircled with a green line in Fig. 6.

Among the remaining  $m_{H^0} \gtrsim 80$  GeV models we find

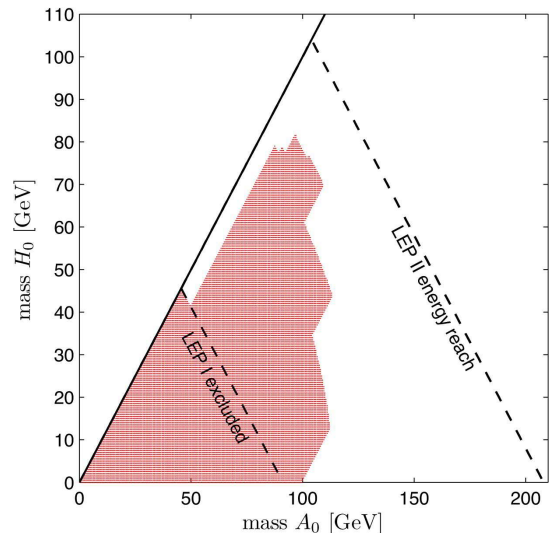


FIG. 7: LEP exclusion plot. The shaded red area indicates the region of the  $(m_{H^0}, m_{A^0})$  plane excluded by LEP data. The lower left triangle, where  $m_{H^0} + m_{A^0} < m_Z$ , is excluded by LEP I data on the Z boson width. The remaining part of the shaded region is excluded by our LEP II analysis. Shown is also the LEP II kinematical limit. Since we are assuming  $m_{H^0} < m_{A^0}$  the upper left region is not accessible.

some for which the ratio between the IDM and MSSM efficiencies drops down to 0.9. We therefore use a factor of 1.1 for the rescaling here, and this region is encircled with a red line in Fig. 6.

Except for in the low  $\Delta m$  and high  $m_{H^0}$  regions mentioned above we find it appropriate to apply the same production limits as for the neutralinos. While this might be argued to be too conservative, the points where harder limits could possibly be imposed are anyway far from excluding any IDM model.

By utilizing the limits on the  $\tilde{\chi}_1^0 \tilde{\chi}_2^0$  production from Fig. 13d) in [16] we find, after rescaling, upper limits on the  $H^0 A^0$  production cross section as a function of  $m_{H^0}$  and  $m_{A^0}$ . The cross section limits, and the regions where we impose rescaling, are found in Fig. 6. Comparing these with the calculated  $e^+ e^- \rightarrow H^0 A^0$  cross sections, which also are shown in Fig. 6, finally tells us which IDM models are excluded.

The resulting exclusion plot is shown in Fig. 7. Roughly speaking, our LEP II analysis exclude models satisfying  $m_{H^0} < 80 \text{ GeV}$ ,  $m_{A^0} < 100 \text{ GeV}$  and  $\Delta m > 8 \text{ GeV}$ . The sharp transition at  $\Delta m = 8 \text{ GeV}$  comes from the steep gradient of the cross section upper limit present in Fig. 13d) in [16].

In [4] it has previously been estimated that the  $H^0 A^0$  production cross section is below the existing LEP II upper limits for models with  $m_{H^0} \approx 70 \text{ GeV}$  and  $\Delta m \lesssim 10 \text{ GeV}$ . We note that our results put somewhat harder constraints in that region. Moreover, [13] presented  $m_{H^0} + m_{A^0} > 130 \text{ GeV}$  as a rule of thumb for models to be consistent with the LEP II data. For  $m_{H^0} > 30$



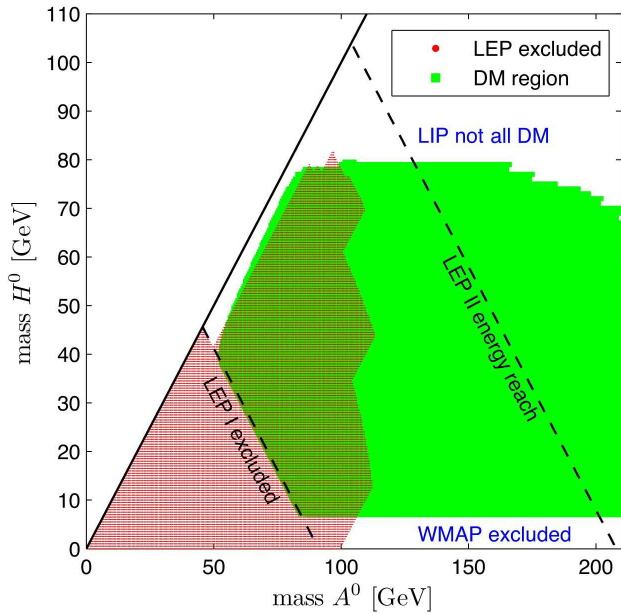


FIG. 8: LEP II limits and dark matter,  $m_h = 200$  GeV. The LEP excluded region of Fig. 7 together with a green region indicating points in the  $(m_{H^0}, m_{A^0})$  plane where there exist models with  $m_h = 200$  GeV capable of providing a good dark matter (DM) candidate  $H^0$  with relic density in agreement with WMAP. Models above the green region are still allowed, but cannot account for all dark matter. Models below the green region leave a relic density higher than the WMAP upper limit, and are hence ruled out.

GeV our analysis hence imposes harder constraints than that.

In order to find out what consequences this LEP II constraint has for  $H^0$  as a dark matter candidate we perform an extensive scan over the IDM parameter space using Darksusy [30] interfaced with FORMCALC [29]. The relic density is calculated, including coannihilations with  $A^0$  and  $H^\pm$ , for models respecting Eqs. (4), (5), (7) and (8) as well as satisfying  $m_{H^\pm} > 70$  GeV [13].

Fig. 8 and Fig. 9 show, for  $m_h = 200$  GeV and  $m_h = 500$  GeV, respectively, the regions where  $H^0$  can have the right relic abundance to account for all dark matter.

Because the only existing (tree level)  $H^0$  self-annihilation channel into fermions is via s-channel  $h$  exchange, models with a heavy  $h$  can only provide a relic density in agreement with the WMAP data if either: 1)  $\Delta m$  is small so that coannihilation with  $A^0$  becomes important, or 2)  $m_{H^0} \sim 75$  GeV so that the efficient annihilations into massive gauge bosons are of just about the right magnitude in the early Universe. If the coannihilations are too strong, or if  $m_{H^0}$  is too large, the relic density will fall below the WMAP lower limit, in which case the model is still allowed but cannot explain all dark matter. These regions are easily identified in Fig. 9.

In Fig. 8 the mass of  $h$  is small enough to allow the  $H^0$  self-annihilating cross section to be large enough to obtain a correct relic density in a larger part of the

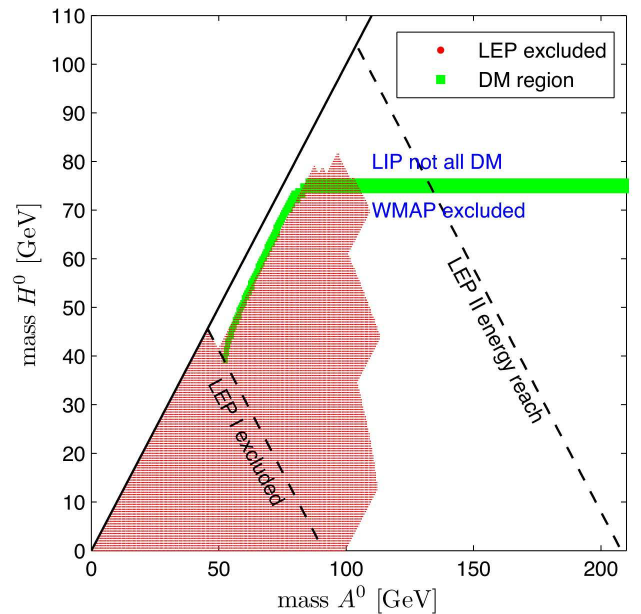


FIG. 9: LEP II limits and dark matter,  $m_h = 500$  GeV. The LEP excluded region of Fig. 7 together with a green band indicating points in the  $(m_{H^0}, m_{A^0})$  plane where there exist models with  $m_h = 500$  GeV capable of providing a good dark matter (DM) candidate  $H^0$  with relic density in agreement with WMAP. Models above the green band are still allowed, but cannot account for all dark matter. Models below the green band all leave a relic density higher than the WMAP upper limit, and are hence ruled out.

$(m_{H^0}, m_{A^0})$  plane. The smaller value of  $m_h$  also allows, because of cancellations between the diagrams contributing to annihilations into massive gauge bosons, for a slightly heavier dark matter candidate  $H^0$ .

As can be seen in Fig. 8 and Fig. 9 the LEP II data can exclude many IDM models of interest from a dark matter perspective, although definitely not all of them.

## V. DISCUSSION

Although we find that appropriate upper limits to impose on the production cross section for inert scalars are similar to those already derived for neutralinos in [16], this result is a priori far from trivial owing to the different properties of the particles.

It is encouraging that the effect of including realistic selection efficiencies is not to invalidate, but rather to increase the confidence in simple applications of limits from other MSSM searches directly onto the IDM. However, one must keep in mind that rather different sets of cuts may be used in other searches, and hence any robust prediction requires an evaluation of the corresponding IDM efficiencies.

One may worry that some of the simplifications used in this analysis misses some important effects. For ex-

ample we do not include any initial state radiation from the incoming  $e^+e^-$  pair. While this is certainly important for the models excluded by LEP I which satisfy  $m_{H^0} + m_{A^0} < m_Z$  (and for which the intermediate s-channel Z bosons can be put on-shell by radiating off photons from the incoming particles) we do not expect the initial state radiation to be very important for our mass range of interest.

Another concern is that the detector generally fails to detect some amount of the energy in high energy jets. On assuming a perfect jet energy determination we indeed find that for models with  $\Delta m \gtrsim 100$  GeV our derived MSSM efficiencies do not match those of [16] as well as they do for lower  $\Delta m$  models. However, by artificially scaling down the jet energy of each event with on average 10-20% before applying the cuts we find good agreements also for these models. An important observation to keep in mind is that we find the ratios between the IDM and MSSM efficiencies to be practically insensitive to the downscaling magnitude. Therefore our final IDM limits do not depend on the very details of the true energy losses. Also, the  $H^0 A^0$  production cross section is in general too low within the high  $\Delta m$  region for any models to be excluded anyway.

In [16] the acoplanar searches were each divided into four subselections (these subselections are the last 1)-4) cuts presented in each of Appendix A and Appendix B). Within their analysis these were treated as independent selections, and we should hence actually check the efficiencies under each of them separately when trying to extract the IDM limits. However, the ratios between our derived IDM and MSSM subselection efficiencies are found to be practically equal to the values for the corresponding complete acoplanar selections. We hence conclude that this does not constitute a problem for our method.

While our analysis certainly includes some approximations, we have consistently been rather conservative in order to minimize the risk of overestimating the final constraints on the IDM. Hence, our derived LEP II limits on the inert scalar masses should be robust.

## VI. SUMMARY

In this paper we have investigated what limits can be inferred on the IDM from an already existing LEP II neutralino search. In performing this translation we have used a method respecting the differences between inert scalars and neutralinos. We have shown that the LEP II data can exclude a significant part of the parameter space, but also that many models providing a good WIMP dark matter candidate still are valid.

## Acknowledgments

We thank Klas Hultqvist for numerous fruitful discussions regarding the analysis of [16] as well as the DELPHI detector in general, for providing us with the lepton identification code, and for careful reading of the manuscript. Thanks also to Anna Lipniacka and Per Johansson for useful comments. E.L. would like to thank Johan Alwall for valuable technical assistance with MADGRAPH/MADEVENT. M.G. is supported by the INFN and the EU FP6 Marie Curie Research & Training Network "UniverseNet" (MRTN-CT-2006-035863). J.E. thanks the Swedish Research Council (VR) for funding support.

## Appendix A

Below follows the acoplanar jets selection cuts we imposed on the quark final states after hadronization in PYTHIA and subsequent rejection of particles lost in the beam pipe (which is taken to cover a polar angle of  $10^\circ$ ). A particle was assumed to carry TPC information if and only if it was more than  $25^\circ$  away from the beam axis. (See [31] for information about the TPC pad rows in the DELPHI detector.) Although some simplifications have been unavoidable, most of our cuts are very close to the original ones. For a list of original cuts see [16].

- A minimum of two charged particles, with at least one of them having a transverse momentum above 1.5 GeV, and a total transverse energy (defined as the sum of the absolute values of the transverse momenta of all individual particles) above 4 GeV, was required.
- At least five charged particles had to carry TPC information.
- The scalar sum of momenta of the particles carrying TPC information had to exceed both 4 GeV and 10% of the total jet energy.
- Exactly two jets were required.
- All jets had to have a polar angle above  $10^\circ$ .
- Each jet had to contain at least one particle with TPC information.
- The particles emitted within  $30^\circ$  of the beam axis had to carry less than 60% of the total jet energy.
- The absolute value of the cosine of the polar angle of the total momentum had to be smaller than 0.9.
- The total transverse momentum (defined as the norm of the vector sum of the individual transverse momenta) had to be larger than 6 GeV.

- The momentum of a jet divided by its energy had to exceed 0.5 for the most energetic jet and 0.4 for the second most energetic jet.
- The total transverse momentum had to be larger than 15 GeV, or the acollinearity (defined as the supplement of the angle between the jets) had to exceed  $40^\circ$ , or the ratio between the momentum and the energy of the second most energetic jet had to be above 0.8.
- If the total transverse momentum was below 12 GeV, the average momentum of the particles with TPC information had to lie between 0.8 GeV and 8 GeV, and the energy of the most energetic neutral particle had to be below 40% of the total jet energy (if the total jet energy exceeded 20 GeV) or below 5 GeV (if the total jet energy was lower than 20 GeV).
- If the total jet energy was below 50 GeV, the average momentum of the particles with TPC information had to lie between 0.8 GeV and 8 GeV, and the momentum of the most energetic charged particles had to lie between 5% and 70% of the total jet energy.
- If the total jet energy was below 20 GeV, the average momentum of the particles with TPC information had to lie between 0.8 GeV and 4 GeV but at least be larger than 20% of the total jet energy, the momentum of the most energetic charged particle had to lie between 10% and 60% of the total jet energy, and the energy of the most energetic neutral particle had to be below 35% of the total jet energy.
- If there were any neutral particles, the norm of the vector sum of the jet momenta and the momentum of the most energetic neutral particle had to exceed 2.5 GeV.
- All neutral particles had to have energies less than 60 GeV.
- All charged particles had to have energies less than 20 GeV.
- The jets had to pass one of the following cuts:
  1. The invariant mass had to be below 10% of  $\sqrt{s}$ , the missing mass had to be above 70% of  $\sqrt{s}$ , the total transverse momentum had to be above 7 GeV, and the scaled acoplanarity (defined as the sine of the minimum angle between a jet and the beam axis times the supplement of the angle between the projections of the jets onto a plane perpendicular to the beam axis) had to exceed  $40^\circ$ .
  2. The invariant mass had to lie between 10% and 30% of  $\sqrt{s}$ , the missing mass had to be above 60% of  $\sqrt{s}$ , the total transverse momentum had to be above 8 GeV, and the scaled acoplanarity had to exceed  $25^\circ$ .
  3. The invariant mass had to lie between 30% and 50% of  $\sqrt{s}$ , the missing mass had to be above 45% of  $\sqrt{s}$ , the total transverse momentum had to lie between 12 GeV and 35 GeV, the total longitudinal momentum (defined as the norm of the vector sum of the individual longitudinal momenta) had to be below 35 GeV, the scaled acoplanarity had to exceed  $25^\circ$ , and the acollinearity had to be lower than  $55^\circ$ .
  4. The invariant mass had to lie between 50% and 70% of  $\sqrt{s}$ , the missing mass had to be above 20% of  $\sqrt{s}$ , the total transverse momentum had to lie between 12 GeV and 35 GeV, the total longitudinal momentum had to be below 35 GeV, the scaled acoplanarity had to exceed  $25^\circ$ , and the acollinearity had to be lower than  $55^\circ$ .

## Appendix B

Below follows the acoplanar leptons selection cuts we imposed on the lepton final states. A particle was assumed to carry TPC information if and only if it was more than  $25^\circ$  away from the beam axis. (See [31] for information about the TPC pad rows in the DELPHI detector.) Although some simplifications have been unavoidable, most of our cuts are very close to the original ones. For a list of original cuts see [16].

- Two leptons needed to be identified.
- At least one of the leptons had to have a transverse momentum above 1.5 GeV, and a total transverse energy above 4 GeV was required.
- Each lepton had to have an energy above 1 GeV.
- Each lepton had to carry TPC information.
- The acoplanarity between the leptons had to be larger than  $10^\circ$ .
- The acollinearity between the leptons had to be larger than  $10^\circ$ .
- The absolute value of the cosine of the polar angle of the total momentum had to be smaller than 0.9.
- The total transverse momentum had to be larger than 6 GeV.
- The leptons emitted within  $30^\circ$  of the beam axis had to carry less than 70% of the total lepton energy.

- If the total transverse energy was below 100 GeV and the total missing momentum was above 45 GeV, then the charge times the cosine of the polar angle of the most energetic lepton was required to be positive.
- If the momentum of the most energetic lepton was between 40 GeV and 100 GeV and the total energy within  $15^\circ$  of this lepton was between 40 GeV and 100 GeV, then the charge times the cosine of the polar angle was required to be greater than -0.65 for both leptons.
- The leptons had to pass one of the following cuts:
  1. The invariant mass had to be below 10% of  $\sqrt{s}$ , the missing mass had to be above 70% of  $\sqrt{s}$ , the total transverse momentum had to be above 7 GeV, and the acoplanarity (defined as the supplement of the angle between the projections of the leptons onto a plane perpendicular to the beam axis) had to exceed  $40^\circ$ .
  2. The invariant mass had to lie between 10% and 30% of  $\sqrt{s}$ , the missing mass had to be above 45% of  $\sqrt{s}$ , the total transverse momentum had to be above 10 GeV, and the acoplanarity had to exceed  $25^\circ$ .
  3. The invariant mass had to lie between 30% and 55% of  $\sqrt{s}$ , the missing mass had to be above 20% of  $\sqrt{s}$ , the total transverse momentum had to be above 12 GeV, and the acoplanarity had to exceed  $15^\circ$ .
  4. The invariant mass had to lie between 55% and 70% of  $\sqrt{s}$ , the missing mass had to be above 20% of  $\sqrt{s}$ , the total transverse momentum had to be above 12 GeV, and the acoplanarity had to exceed  $15^\circ$ .

- 
- [1] N. G. Deshpande and E. Ma, Phys. Rev. D **18**, 2574 (1978).
- [2] E. Ma, Phys. Rev. D **73**, 077301 (2006) [hep-ph/0601225].
- [3] E. Ma, Mod. Phys. Lett. A **21**, 1777 (2006) [hep-ph/0605180].
- [4] R. Barbieri, L. J. Hall and V. S. Rychkov, Phys. Rev. D **74**, 015007 (2006) [hep-ph/0603188].
- [5] Q. H. Cao, E. Ma and G. Rajasekaran, Phys. Rev. D **76**, 095011 (2007) [arXiv:0708.2939 [hep-ph]].
- [6] J. A. Casas, J. R. Espinosa and I. Hidalgo, Nucl. Phys. B **777**, 226 (2007) [hep-ph/0607279].
- [7] T. Hambye and M. H. G. Tytgat, Phys. Lett. B **659**, 651 (2008) [arXiv:0707.0633 [hep-ph]].
- [8] L. Lopez Honorez, E. Nezri, J. L. Oliver and M. H. G. Tytgat, JCAP **0702**, 028 (2007) [hep-ph/0612275].
- [9] M. Gustafsson, E. Lundström, L. Bergström and J. Edsjö, Phys. Rev. Lett. **99**, 041301 (2007) [arXiv:astro-ph/0703512].
- [10] D. N. Spergel *et al.*, Astrophys. J. Suppl. Ser. **170**, 377 (2007) [astro-ph/0603449].
- [11] E. Komatsu *et al.* [WMAP Collaboration], arXiv:0803.0547 [astro-ph].
- [12] LEP Electroweak Working Group, status of July 2008, <http://lepewwg.web.cern.ch/LEPEWWG/>.
- [13] A. Pierce and J. Thaler, JHEP **0708**, 026 (2007) [arXiv:hep-ph/0703056].
- [14] E. Ma, Phys. Lett. B **659**, 885 (2008) [arXiv:0710.2325 [hep-ph]].
- [15] P. D. Serpico and G. Zaharijas, Astropart. Phys. **29** (2008) 380 [arXiv:0802.3245 [astro-ph]].
- [16] M. Espirito Santo, K. Hultqvist, P. Johansson, A. Lipniacka, DELPHI 2003-002 PHYS 928 (2003), <http://delphiwww.cern.ch/pubxx/delnote/dn2003.html>.
- [17] Fermi Gamma-ray Space Telescope, <http://www-glast.stanford.edu/>.
- [18] M. Acciarri *et al.* [L3 Collaboration], Phys. Lett. B **472**, 420 (2000) [arXiv:hep-ex/9910007].
- [19] R. Barate *et al.* [ALEPH Collaboration], Phys. Lett. B **499**, 67 (2001) [arXiv:hep-ex/0011047].
- [20] J. Abdallah *et al.* [DELPHI Collaboration], Eur. Phys. J. C **31**, 421 (2004) [arXiv:hep-ex/0311019].
- [21] G. Abbiendi *et al.* [OPAL Collaboration], Eur. Phys. J. C **35**, 1 (2004) [arXiv:hep-ex/0401026].
- [22] J. Alwall *et al.*, JHEP **0709**, 028 (2007) [arXiv:0706.2334 [hep-ph]].
- [23] G. A. Moortgat-Pick and H. Fraas, Phys. Rev. D **59**, 015016 (1999) [arXiv:hep-ph/9708481].
- [24] S. Katsanevas and P. Morawitz, Comput. Phys. Commun. **112**, 227 (1998) [arXiv:hep-ph/9711417].
- [25] T. Sjöstrand, Comput. Phys. Commun. **82**, 74 (1994).
- [26] T. Sjöstrand, S. Mrenna and P. Skands, JHEP **0605**, 026 (2006) [arXiv:hep-ph/0603175].
- [27] K. Hultqvist, private communication.
- [28] A. Djouadi, J. L. Kneur and G. Moultaka, Comput. Phys. Commun. **176**, 426 (2007) [arXiv:hep-ph/0211331].
- [29] T. Hahn and M. Perez-Victoria, Comput. Phys. Commun. **118**, 153 (1999) [hep-ph/9807565]; T. Hahn, Comput. Phys. Commun. **140**, 418 (2001) [hep-ph/0012260].
- [30] P. Gondolo, J. Edsjö, P. Ullio, L. Bergström, M. Schelke and E. A. Baltz, JCAP **0407**, 008 (2004) [astro-ph/0406204].
- [31] P. Abreu *et al.* [DELPHI Collaboration], Nucl. Instrum. Meth. A **378**, 57 (1996).